NASA Technical Memorandum 79017

CRITICAL MASS FLUX THROUGH SHORT BORDA TYPE INLETS OF VARIOUS CROSS SECTIONS

R. C. Hendricks
Lewis Research Center
Cleveland, Ohio 44135

and

N. P. Poolos
Lake Ridge Academy
North Ridgeville, Ohio

TECHNICAL PAPER to be presented at the
Fifteenth International Congress of Refrigeration
sponsored by the International Institute of Refrigeration
Venice, Italy, September 23-29, 1979

CRITICAL MASS FLUX THROUGH SHORT BORDA TYPE INLETS OF VARIOUS CROSS SECTIONS

R. C. Hendricks
NASA Lewis Research Center
Cleveland, Ohio 44135

and

N. P. Poolos*
Lake Ridge Academy
North Ridgeville, Ohio

Mass flux measurements associated with choked flows through four Borda type inlet geometries: circular, square, triangular and rectangular (two-dimensional) and two sharp edged geometries taken over a very wide range of inlet stagnation conditions indicate:

(1) The mass flux is independent of the inlet cross-section geometry

(2) The mass flux is dependent only on the inlet stagnation conditions.

Also by using choked flow results found in the literature, the reduced mass flux is independent of working fluid.

Two implications are drawn which remain to be verified: (1) since seal leak rates are weakly dependent on geometry but pressure distribution is strongly dependent on geometry, seal design efforts should be directed more toward controlling the dynamics, (2) high-L/D ducts of arbitrary cross section and Borda type inlets can possess free jets.

E-9868

INTRODUCTION

In the design of heat exchangers, seals, shaft dampers and bearings one is often required to minimize losses which requires optional geometric configurations. As such inlet geometry both parallel and normal to the flow field often becomes a critical factor.

It has been shown that the mass flux through two-dimensional and axisymmetric nozzles is independent of geometry for two phase choked flow references 1 and 2. In reference 3 the orifice geometry was studied over a wide range in fluid conditions and related to the nozzle. The problem of predicting mass flux for other fluids based on theory and data for a given fluid was resolved in references 4, 5, and 6. Since one dimensional theory was used to correlate data of references 1 to 6, it is reasonable to assume that the critical mass flux is independent of geometry and the above results apply without modification.

---

* Current address: University School, Chagrin Falls, Ohio.

Recently Hendricks and Simoneau, reference 7, assessed some effects of a configuration parallel to the flow on mass flux and pressure distribution using a 53 L/D tube with a Borda type inlet. It was found that the axial pressure distribution is very sensitive to inlet stagnation conditions. The major phenomena occurring in the tube are illustrated on figure 1. A conventional gas choked flow pressure profile serves as reference. The remaining profiles are for fluid nitrogen holding stagnation conditions nearly constant while increasing the back pressure. For a low back pressure at the exit, the pressure drops abruptly at the entrance to a level near the fluid saturation pressure and some fluid vaporizes. Subsequently, the fluid recompresses slightly and then traverses the entire length of the tube at nearly constant pressure, actually showing a small pressure rise. Increases in back pressure to nearly 0.4 P_0 have little effect on these profiles or the flow rate. The flow is choked. As the back pressure is increased a zone of secondary recompression forms within the tube. This is most clear for the profile with the triangular symbols. This is most clear for the profile with the triangular symbols. This is analogous to a moving shock up in a diffuser in single phase choked flow; however, here the flow cross-section is a constant area tube. At back pressures near 0.5 P_0 the secondary recompression zone moves to the inlet and finally unchokes the flow. The flow chokes at the tube entrance rather than the exit. Variation of stagnation conditions offer a more complex picture and it appears that fluid jetting cannot be sustained for stagnation conditions much beyond the thermodynamic critical point. While the authors of reference 7 presented no theoretical solution, an empirical expression was given to predict conditions under which the zone of secondary recompression will occur within the tube (or where jetting can take place)

$$P_R = c(L/D,\epsilon)\ T_R^7 \qquad (1)$$

Although the axial pressure profiles are changed significantly near this locus, there appears to be little, if any, effect on mass flow rate.

This contrast in pressure profiles can present serious design problems especially for parallel surfaces as found in seals, bearings, and heat exchanger tubes of rectangular cross-section with Borda type inlet configurations. As will be shown such configurations can be subjected to very large forces. However such profiles can be beneficial in other designs such as ejectors, jet pumps, cutters and refrigerators where jetting is desirable.

In this paper we will examine how the critical mass

flux depends on inlet cross section geometry by comparing the results obtained with four different inlet cross sections: circular, square, rectangular, triangular. And by combining data and theories of the literature, extend these results to other geometries and fluids.

FLOW MODEL

While all inlet geometries are susceptible to separation under some conditions, some geometries such as sharp edged and Borda are most susceptible to separation.

The type of separation phenomena encountered at the inlet to the Borda configuration results from a discontinuity in the slope of the bounding surface see fig. 2. As the streamline cannot conform to the bounding surface, it separates and subsequent growth or decay of the disturbance depends on the degree of discontinuity (see fig. 2). Theoretically the Borda inlet causes a full reversal of the streamline and as such represents the strongest discontinuity for simple geomtries.

The geometry of the free streamline in potential flow is found by integrating the real and imaginary components of dz reference 9 (see fig. 2).

$$z = x + iy = \frac{1}{V_0} \int V_0 \frac{dz}{dw}\, dw \tag{2}$$

The free streamline can be defined in terms of the parameter θ, where θ ranges from 0 to π:

$$x_0 = \frac{2x}{B} - \frac{1}{\pi}\left\{\sin^2\left(\frac{\theta}{2}\right) + \log\left[\cos\left(\frac{\theta}{2}\right)\right]\right\} \tag{3}$$

$$y_0 = \frac{4y}{B} = \frac{1}{\pi}\left(2\pi - \theta \sin\theta\right) \tag{4}$$

While the above applies to the two-dimensional case (fig. 2(a)), it can be shown that similar streamlines exist for the axisymmetric case reference 9, however the problem for a general cross section was not solved. Suggested streamlines for other geometric configurations are shown in figure 3, where soap films and associated sketches represent potential interfaces and by analogy separated interfaces.

From momentum considerations one can establish A_2/A_1 reference 8 and 9. The control surface consists of the Borda walls, the free jet surface, a normal cross-section through the jet at "infinity" and an

"infinite" spherical surface over the inlet (see fig. 2). The flow in the choked free jet was found to equalize a short distance from the inlet (ref. 9).

The available momentum of the jet per unit time is $P_0 A_1$. The available potential energy is $P_0 V_j$ where V_j is the jet volume. The momentum of the jet is $\rho V_j U_j$; its kinetic energy is $1/2\,\rho V_j U_j^2$. Here $V_j = U_j A_2$ and it follows that

$$P_0 A_1 = \rho A_2 U_j^2 \tag{5}$$

$$P_0 A_2 U_j = \frac{1}{2}\rho A_2 U_j^3 \tag{6}$$

Eliminating P_0 gives

$$A_2/A_1 = 1/2 \tag{7}$$

It is important to note here that for both the axisymmetric and two dimensional cases $A_2/A_1 = 1/2$.

Thus while the argument is quite simple, where combined with the above cases, it makes an important point: the contraction area ratio could be independent of cross-section geometries such as circular, square, rectangular and triangular. Thus it should follow that mass flux through Borda inlets is independent of cross section geometry, or to a first order,

$$\left.\frac{A_{flow}}{A_{inlet}}\right|_{\substack{\text{Borda}\\ \text{Inlet}}} = \text{Constant} \tag{8}$$

Further, using references 4 to 6, critical mass flux should be completely characterized by inlet stagnation conditions. These concepts will be established in the subsequent sections.

APPARATUS AND INSTRUMENTATION

The general scheme of the apparatus follows that described in reference 7. The basic flow facility (see fig. 4) was of the blow-down type where flow rates were metered using a venturi flowmeter in the bottom of the storage tank. Gas flow rates were metered using the orifice flowmeter in the exhaust stack. Inlet stagnation conditions were

measured in a mixing chamber immediately upstream of the test section. The installed test section with approach and downstream pressure taps is shown as figure 5, with the characteristic dimensions of each test geometry illustrated as figure 6.

The four basic Borda type inlet geometries: circular, square, rectangular (2D) and triangular are pictured in figure 7. Two associated geometries the thick and thin orifices are shown in figure 8.

The flow areas of each geometry are given in table I; they are approximately equal. It was found that the internal surface of the rectangular inlet was slightly concave-convex, i.e., venturi like, by approximately 0.007 mm; as such it may give slightly larger flow rates than flat parallel surfaces.

RESULTS

As a reference for discussion, the isentropic reduced mass flux for nozzles is given as figure 9, from reference 10:

$$G_{R_I} = G_I/G^* \tag{9}$$

For each of the four Borda Inlets data were taken along four stagnation temperature isotherms, nominally T_{R_0}=0.68, 0.90, 1.01, 1.31. Gas data were also taken. These results are presented as figures 10 to 13. For the thick and thin orifices, one isotherm T_{R_0}=0.68 and gas data were taken.

Circular Inlet

The reduced mass flux data for the circular inlet configuration as a function of reduced stagnation pressure for the four selected isotherms and gas are shown on figure 10. The data are presented in table II. Points on the 0.90 isotherm appear to have more scatter than those on adjacent isotherms which can be related to operational difficulties in setting these conditions. The two points at 0.5 reduced pressure appear as saturation data, and may have saturated conditions at the inlet.

Square Inlet

The reduced mass flux data for the square inlet Borda configuration are given as figure 11. The data are given in table III. Due to an overload on the flow differential pressure transducers for two points, readings from static transducers had to be used. The data lie on the curve, but must be considered questionable.

Triangular Inlet

The reduced mass flux data for the triangular inlet Borda geometry are given as figure 12. The data are given as table IV. In general we did not seek saturated data points, but the point on the $T_{R_0} = 0.9$ locus at $P_{R_0} \sim 0.6$ is quite close to saturation.

Rectangular Inlet

The reduced mass flux data for the rectangular inlet Borda geometry are given as figure 13 and the data presented as table V. This geometry has an aspect ratio of 4 and can be classified as nearly two dimensional. Again we have two saturated points along the $T_{R_0} = 0.9$ isotherm. As noted in the apparatus section, this geometry is shaped slightly like a venturi.

Comparison of Data

A direct comparison of data for the four Borda geometries is difficult. However, using nominal isotherms, figures 10 to 13 were overlayed to construct figure 14. A comparison of these curves reveals little difference in reduced mass flux over a very large range of inlet stagnation conditions. Figure 14 demonstrates that even for the complex triangular inlet, the reduced mass flux is independent of cross section geometry. But it should be noted that the rectangular inlet shows a possible 2 percent increase in mass flux, see the $T_{R_0} = 0.68$ isotherm, figure 14.

Thick Orifice

The geometry of the thick orifice may be considered a short tube, with $L/D = 2$, similar to the circular Borda geometry except that the entrance is sharp edged, i.e., does not protrude into the flow.

The data for the $T_{R_0} = 0.68$ isotherm and gas for this geometry is given as table VI and shown on figure 15. When compared to the isentropic nozzle, the flow coefficient would be 0.66. These results are about 5 percent above those of the Borda inlets about 5 to 7 percent above those of reference 3 and about 18 percent above the 53 L/D-Borda inlet of reference 7.

Thin Orifice

Shortening the orifice length to $L/D = 2/3$ reduced the mass flux by about 5 percent or nearly equivalent to that of the Borda inlets, see figure 15, and table VII. The results are also in good agreement with those of reference 3. The gaseous data for, thin or thick orifice or Borda inlets are

nearly all the same on this figure.

These data, of course, indicate a separation problem at the inlet of the sharp edged configuration of proportions nearly equal to that of the Borda configurations. This implication remains to be resolved.

Comparison to Theory

In reference 3 orifice data were compared to analytical preductions using a flow coefficient (no further comparison of orifice data need be made). Herein we use the same approach and define a coefficient which is the ratio of the experimental to calculated mass flux:

$$C_0\left(P_{R_0},\ T_{R_0}\right) = \frac{GR}{GR_I} \tag{10}$$

In reference 7, using an extensive data set for a 53 L/D Borda tube, a Co locus was established. The data of this paper are compared to that locus established in figure 16. It should follow that all Borda inlets circular, square, triangular, rectangular, etc., will approximate the dashed locus in a manner similar to the solid locus of reference 7; however conditions where the stagnation temperatures are close to the thermodynamic critical point remain unclear.

Discussion

These Borda inlet data for critical mass flux indicate that (see fig. 1(a)):

(1) A_2/A_1 = constant, independent of inlet cross section geometry for a given inlet stagnation condition

(2) G_R is also independent of cross section geometries of equal areas and completely characterized by inlet stagnation conditions.

Also when combined with previous investigations references 4 to 6 these results can be extended to any corresponding states fluid.

The data also suggest that parallel surfaces as found in seals, dampers, bearings, and heat exchanger tubes of rectangular cross section with Borda type inlet configurations are subject to very large forces*

(1) tubes of insufficient strength can be readily collapsed fully or partially when separation occurs; in such cases severe flow blockage occurs and metal to metal contact

---

*This is true for all geometries; however due to the high aspect ratio of the rectangle, deformations can be readily detected.

is imminent.

(2) separated flows are not steady, they oscillate; such perturbations can be destructive over a period of time and certainly can make the inlet "sing."

As an illustration of the magnitude of such forces one only has to consult the data tables, compare the upstream and downstream pressures and recall the model of figure 7. In reference 7 it was shown that the ratio of $P_0/P_B > 125$.

Implications for Larger L/D Channels

The results of this experiment can be extended to yield insight on two items of importance in larger channels. Since flow rates are unaffected by cross section geometry, circular, square, triangular, rectangular and the data of reference 7 are for a 53 L/D circular Borda tube, it is implied that the data of reference 7 can be extended to large L/D ducts of arbitrary cross section with Borda type inlets. First they can prossess free jet effects as reported in reference 7. Second, recompression of the free jet also has little effect on mass flux on the other hand, the pressure profiles in larger L/D ducts are of major significance and are greatly dependent on the location of the recompression zone. Thus the work in seals and bearings and heat exchangers should be directed more toward control of the dynamics as the pressure profile is strongly dependent on geometry, and the leak rates are weakly dependent on geometry.

ACKNOWLEDGEMENT

The assistance of J. A. Hendricks and J. R. Hendricks in preparing this document is greatly appreciated.

SUMMARY

A comparison of data and/or the figures herein demonstrates the original thesis that for these Borda inlet geometries: circular, square, triangular, and rectangular (2-dimensional),

(1) The mass flux is independent of inlet cross section

(2) The choked mass flux is dependent only on the inlet stagnation conditions

Also by using the reduced mass flux and the principal of corresponding states given in references 4 to 6, the reduced mass flux is independent of the working fluid.

The importance of these items make it quite clear that mass flux values obtained for circular inlets apply to any other type of simple cross sections and implications are that these results are quite universal for a variety of fluids over a very large range in inlet conditions. Furthermore there is some evidence that these same constraints will apply to the sharp edged geometries.

Combining the results herein with those of reference 7, the implication in seals and heat exchanger designs are clear; with mass flux (leak rates) weakly dependent and pressure profiles highly dependent on inlet geometry, it would appear that seal design efforts should concentrate on those geometries most amenable to dynamic stability.

SYMBOLS

A	area, cm
B	slot or channel width, cm
C_0	flow coefficient, eq. (10)
D	tube diameter, cm
G	flow rate, g/cm^2-s
G_R=G/G*	reduced flow rate
G*	flow normalizing parameter, $\sqrt{P_c\rho_c/Z_c}$, 6010 g/cm^2-s, for nitrogen
L	tube length, cm
P	pressure MPa
P_R	reduced pressure, P/P_c
R	gas constant, MPa-cm^3/g-K
T	temperature, K
T_R	reduced temperature, T/T_c
U	velocity, cm/sec
V	specific volume, cm^3/g
V	velocity parameter
w	complex potential
X	distance, cm
x	dimensionless distance
Y	distance,cm
y	dimensionless distance
Z	compressibility, PV/RT
z	complex coordinate, cm
ρ	density, g/cm^3

Subscripts:

c	critical
I	isentropic
0	stagnation
j	jet
1,2	reference conditions
H	hydraulic

REFERENCES

1. Simoneau, R. J. and Hendricks, R. C., 'Two-Phase Choked Flow of Cryogenic Fluids in Converging-Diverging Nozzles,' proposed NASA Technical Publication.
2. Simoneau, R. J., 'Two-Phase Choked Flow of Subcooled Nitrogen through a Slit', Proceedings of the Tenth Southeastern Seminar on Thermal Sciences, (1974) also NASA TM X-71516 (1974).
3. Simoneau, R. J., "Maximum Two Phase Flow Rates of Subcooled Nitrogen through a Sharp-Edged Orifice," Advances in Cryogenic Engineering, Vol. 21, Timmerhaus, K. D. and Weitzel, D. H., (eds.), Plenum Press, New York, (1975', pp. 299-306.
4. Hendricks, R. C., 'Normalizing Parameters for the Critical Flow Rate of Simple Fluids through Nozzle', Proc. Fifth International Cryogenic Engineering Conference (1974), Paper J10, pp. 278-281.
5. Hendricks, R. C. and Simoneau, R. J., 'Application of the Principle of Corresponding States to Two-Phase Choked Flow', Presented at the 74th National AIChE Meeting, (1973) also NASA TM X-68193 (1973).
6. Hendricks, R. L., Simoneau, R. J. and Barrows, R. F., 'Two-Phase Choked Flow of Subcooled Oxygen and Nitrogen', NASA TN D-8149 (1976).
7. Hendricks, R. C. and Simoneau, R. J., 'Some Flow Phenomena in a Constant Area Duct with a Borda Type Inlet', NASA TM-78943 (1978).
8. Birkhoff, G. and Zarantonello, E. H., Jets, Wakes and Cavities Applied Mathematics and Mechanics, Vol. II, Academic Press, New York (1957).
9. Gurevich, M. I., Theory of Jets in Ideal Fluids, Academic Press, New York (1965).
10. Simoneau, R. J. and Hendricks, R. C., 'Generalized Charts for Computation of Two-Phase Choked Flow of Simple Cryogenic Liquids', Cryogenics, Vol. 17 (1977), pp. 73-76.

TABLE I. - SUMMARY OF KEY GEOMETRIC

FEATURES OF TEST SECTIONS

Inlet cross section geometry	Type	Flow area (cm^2)	L/D_H	G^*A (g/sec)
Circular	Borda	0.1810	2	1088
Square	Borda	.1789	2.25	1075
Rectangular	Borda	.1858	2.75	111
Triangular	Borda	.1966	2.45	[illegible]
Circular	Sharp edge	.1791	2	1076
Circular	Sharp edge	.1800	2/3	1082

TABLE II. - FLOW DATA FOR CIRCULAR BORDA INLET

RUN	FLOW G/SEC	TEMP K	PIN MPA	POUT MPA	PBACK MPA	RUN	FLOW G/SEC	TEMP K	PIN MPA	POUT MPA	PBACK MPA
1953	73.0	254.8	1.69	0.19	0.22	1971	206.0	144.0	3.21	0.35	0.35
1954	128.0	261.5	3.05	0.32	0.33	1972	116.0	143.8	1.90	0.23	0.25
1955	187.0	266.8	4.47	0.42	0.44	1973	104.0	144.9	1.75	0.21	0.24
1956	243.0	272.5	5.90	0.54	0.57	1974	971.0	113.4	6.59	0.54	0.76
1957	242.0	276.4	7.14	0.64	0.67	1975	853.0	113.6	5.35	0.54	0.66
1958	1098.0	84.9	6.46	0.09	0.40	1976	707.0	113.5	3.93	0.54	0.57
1959	968.0	84.9	5.12	0.09	0.32	1977	554.0	114.1	2.79	0.52	0.49
1960	849.0	85.2	3.95	0.13	0.29	1978	384.0	113.2	1.74	0.44	0.37
1961	687.0	85.4	2.71	0.15	0.26	1979	285.0	126.1	3.28	0.43	0.39
1962	522.0	84.6	1.62	0.16	0.24	1980	281.0	126.7	3.39	0.43	0.40
1963	966.0	112.8	6.49	0.53	0.76	1981	122.0	127.4	1.86	0.23	0.25
1964	915.0	117.2	6.33	0.60	0.75	1982	807.0	127.1	6.67	0.84	0.85
1965	805.0	116.5	5.15	0.60	0.67	1983	672.0	126.6	5.52	0.74	0.68
1966	685.0	115.7	3.95	0.57	0.58	1984	514.0	126.4	4.42	0.61	0.55
1967	563.0	114.8	2.90	0.53	0.50	1985	302.0	126.3	3.35	0.44	0.40
1968	308.0	113.4	1.74	0.37	0.32	1986	150.0	126.6	2.26	0.27	0.27
1969	470.0	144.4	6.07	0.66	0.63	1987	68.0	127.4	1.11	0.15	0.19
1970	334.0	143.8	4.83	0.52	0.51						

TABLE III. - FLOW DATA FOR SQUARE BORDA INLET

RUN	FLOW G/SEC	TEMP K	PIN MPA	POUT MPA	PBACK MPA	RUN	FLOW G/SEC	TEMP K	PIN MPA	POUT MPA	PBACK MPA
1851	800.6	85.6	7.31	0.06	0.45	1876	286.7	286.7	7.33	1.89	2.21
1852	935.7	85.2	4.75	0.09	0.33	1877	288.2	286.5	7.33	1.07	1.24
1853	698.8	85.2	2.95	0.12	0.29	1878	287.8	286.4	7.33	0.72	0.66
1854	530.1	84.6	1.84	0.13	0.25	1879	1124.0	84.4	6.53	0.06	0.37
1855	415.7	84.6	1.28	0.15	0.23	1880	989.8	84.6	5.29	0.07	0.29
1856	717.2	117.1	7.48	0.62	0.81	1881	844.2	84.7	3.94	0.09	0.26
1857	688.5	116.5	5.55	0.61	0.70	1882	718.2	84.9	2.99	0.09	0.25
1858	568.5	115.0	3.26	0.54	0.52	1883	548.5	84.4	1.76	0.09	0.23
1859	376.7	113.7	1.96	0.44	0.40	1884	480.4	112.5	6.58	0.55	0.74
1860	531.5	140.5	5.69	0.55	0.61	1885	856.1	112.7	5.45	0.54	0.64
1861	292.3	133.2	4.13	0.39	0.44	1886	713.3	112.7	4.12	0.54	0.56
1862	183.3	123.6	2.89	0.33	0.34	1887	554.7	114.1	2.94	0.52	0.47
1863	105.7	117.8	1.90	0.23	0.25	1888	326.4	112.9	1.72	0.38	0.32
1864	373.0	177.6	5.73	0.58	0.54	1889	803.2	128.9	6.70	0.75	0.76
1865	375.1	179.1	5.74	0.59	0.55	1890	647.0	127.8	5.54	0.67	0.65
1866	179.2	166.3	3.58	0.39	0.38	1891	493.2	127.5	4.50	0.56	0.53
1867	97.1	157.1	2.07	0.26	0.26	1892	259.0	126.8	3.39	0.41	0.37
1868	66.6	150.1	1.50	0.21	0.22	1893	98.5	132.3	1.69	0.22	0.21
1869	63.8	[illegible]	1.63	0.22	0.21	1894	890.6	127.1	6.99	0.79	0.84
1870	114.7	291.1	2.88	0.31	0.30	1895	719.4	145.0	7.38	0.69	0.77
1871	178.7	286.2	4.58	0.46	0.43	1896	447.4	144.8	5.90	0.53	0.60
1872	231.4	287.5	5.94	0.58	0.55	1897	261.8	144.6	4.10	0.42	0.42
1873	285.6	289.6	7.32	0.72	0.66	1898	134.1	145.1	2.34	0.28	0.26
1874	287.8	287.6	7.33	2.78	3.04	1899	54.8	187.6	2.91	0.31	0.29
1875	286.5	287.1	7.33	3.22	3.47	0	0.0	0.0	0.10	0.10	0.10

TABLE IV. - FLOW DATA FOR TRIANGULAR BORDA INLET

RUN	FLOW G/SEC	TEMP K	PIN MPA	POUT MPA	PBACK MPA	RUN	FLOW G/SEC	TEMP K	PIN MPA	POUT MPA	PBACK MPA
1900	82.0	262.4	1.84	0.25	0.21	1912	798.0	114.0	4.31	0.58	0.61
1901	134.0	269.0	3.00	0.37	0.31	1913	623.0	113.6	3.02	0.55	0.49
1902	197.0	274.0	4.48	0.53	0.44	1914	391.0	115.1	1.99	0.47	0.36
1903	249.0	278.2	5.70	0.66	0.55	1915	885.0	127.4	6.78	1.09	0.93
1904	304.0	283.0	7.04	0.81	0.68	1916	594.0	127.2	4.70	0.77	0.62
1905	1162.0	84.6	5.98	0.07	0.42	1917	514.0	127.5	4.33	0.69	0.55
1906	1053.0	84.6	4.96	0.07	0.29	1918	327.0	126.8	3.42	0.49	0.40
1907	916.0	84.6	3.79	0.09	0.25	1919	667.0	142.7	7.16	0.96	0.80
1908	748.4	84.8	2.60	0.13	0.23	1920	499.0	141.9	5.83	0.79	0.64
1909	564.0	84.1	1.53	0.15	0.20	1921	301.0	142.6	4.14	0.53	0.44
1910	1092.0	114.6	7.22	0.57	0.80	1922	131.0	129.0	1.88	0.27	0.22
1911	987.0	114.7	6.14	0.58	0.74	1923	87.0	144.2	1.37	0.21	0.17

TABLE V. - FLOW DATA FOR RECTANGULAR BORDA INLET

RUN	FLOW G/SEC	TEMP K	PIN MPA	POUT MPA	PBACK MPA	RUN	FLOW G/SEC	TEMP K	PIN MPA	POUT MPA	PBACK MPA
1924	90.7	256.0	2.04	0.20	0.25	1939	575.0	114.3	2.95	0.62	0.56
1925	135.3	263.1	3.13	0.27	0.34	1940	803.0	128.8	6.72	0.84	0.82
1926	194.7	268.6	4.61	0.37	0.46	1941	668.0	128.0	5.66	0.73	0.71
1927	242.1	275.3	5.82	0.46	0.57	1942	359.0	127.8	3.73	0.45	0.44
1928	296.6	280.3	7.16	0.55	0.68	1943	187.0	126.8	2.63	0.25	0.32
1929	1197.8	85.1	6.99	0.14	0.43	1944	983.0	114.1	6.42	0.63	0.77
1930	1114.0	85.3	6.12	0.13	0.35	1945	862.0	113.6	5.13	0.62	0.67
1931	994.0	85.6	4.93	0.14	0.29	1946	414.0	114.3	2.04	0.47	0.39
1932	871.0	85.7	3.80	0.14	0.28	1947	256.0	113.7	1.75	0.30	0.29
1933	725.0	86.0	2.68	0.16	0.26	1948	276.0	114.2	1.82	0.33	0.31
1934	557.0	85.2	1.64	0.16	0.23	1949	610.0	142.9	7.01	0.71	0.76
1935	976.0	114.6	6.40	0.64	0.78	1950	480.0	143.1	5.99	0.58	0.64
1936	844.0	113.8	5.00	0.61	0.66	1951	318.0	143.4	4.53	0.39	0.47
1937	726.0	113.5	3.95	0.59	0.58	1952	128.0	143.2	2.09	0.22	0.26
1938	258.0	113.8	1.76	0.30	0.28						

TABLE VI. - THICK ORIFICE

CHOKED FLOW DATA

Liquid data

Run	$\dot{\omega}$	T_{IN}	P_{IN}	
1258	1185.	85.4	7.13	Thick orifice
1259	985.	85.3	5.03	
1260	740.	85.3	2.92	
1261	575.	84.3	1.80	
1262	1116.	84.7	6.28	
1263	874.	84.4	3.91	
1264	655.	83.7	2.28	
1265	511.	83.5	1.46	

Gas data

1323	82.	273.2	2.05	Thick orifice
1329	124.	274.9	3.07	
1330	181.	274.8	4.45	
1331	234.	275.1	5.72	
1332	292.	275.7	7.10	

TABLE VII. - THIN ORIFICE

CHOKED FLOW DATA

Liquid data

Run	$\dot{\omega}$	T_{IN}	P_{IN}	
1283	1148.	84.9	7.37	Thin orifice
1284	957.	84.6	5.21	
1286	536.	83.7	1.75	
1287	1049.	84.3	6.19	
1288	835.	84.0	3.98	
1289	621.	83.4	2.28	
1290	462.	83.3	1.34	

Gas data

1313	82.	245.7	2.04	Thin orifice
1314	124.	256.0	3.10	
1315	179.	260.8	4.51	
1316	235.	263.6	5.92	
1317	290.	265.9	7.34	

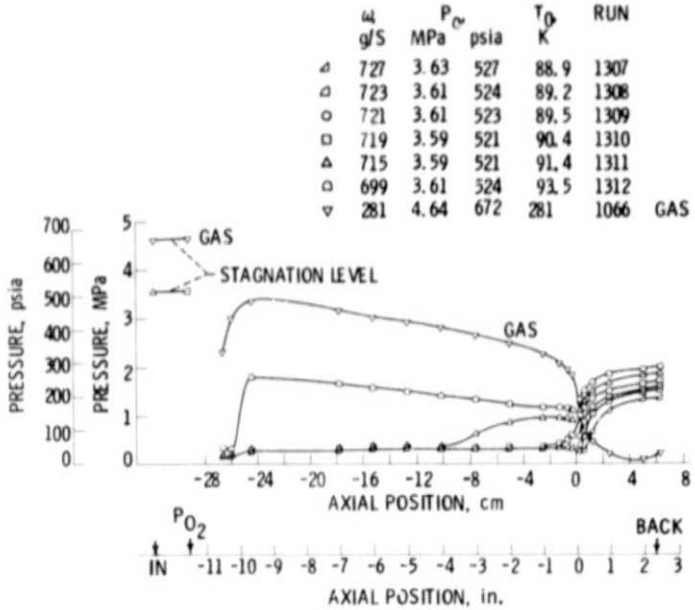

Figure 1. - Typical pressure profiles - axial position 53 L/D straight tube with Borda inlet. From reference 7.

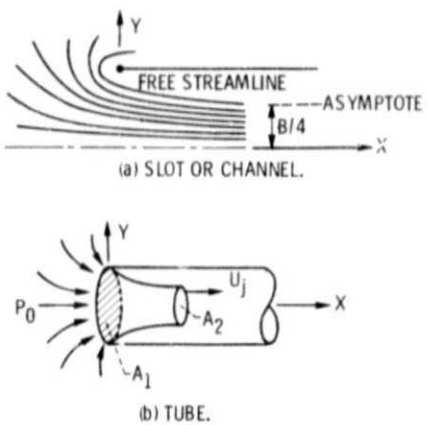

Figure 2. - Schematic for theoretical streamlines for a Borda inlet.

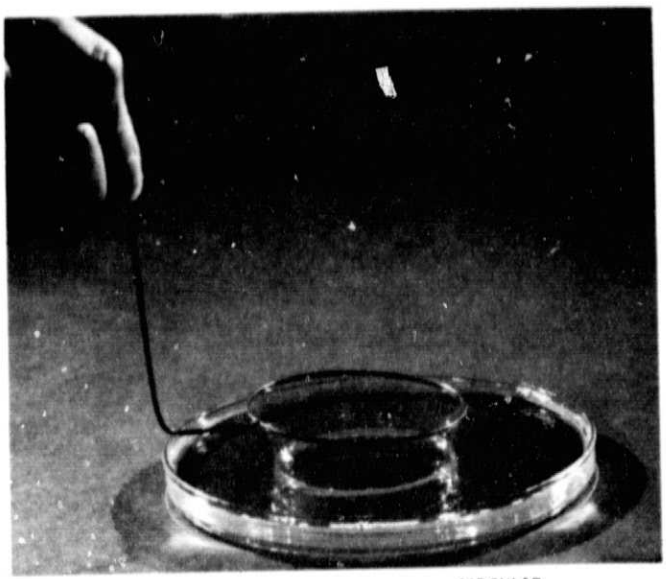

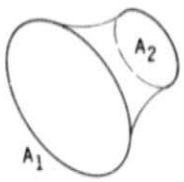

CIRCULAR

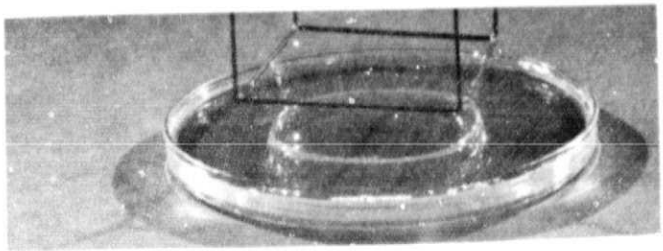

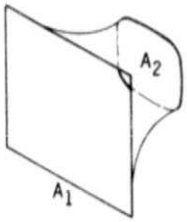

SQUARE

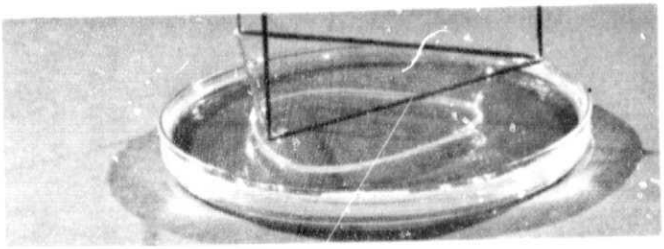

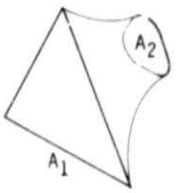

TRIANGULAR

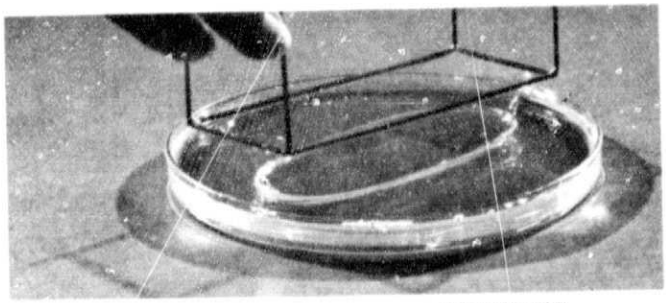

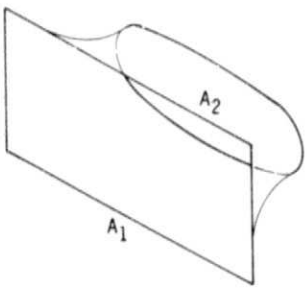

RECTANGULAR

Figure 3. - Soap film simulations and associated sketches of potential flow in Borda inlets.

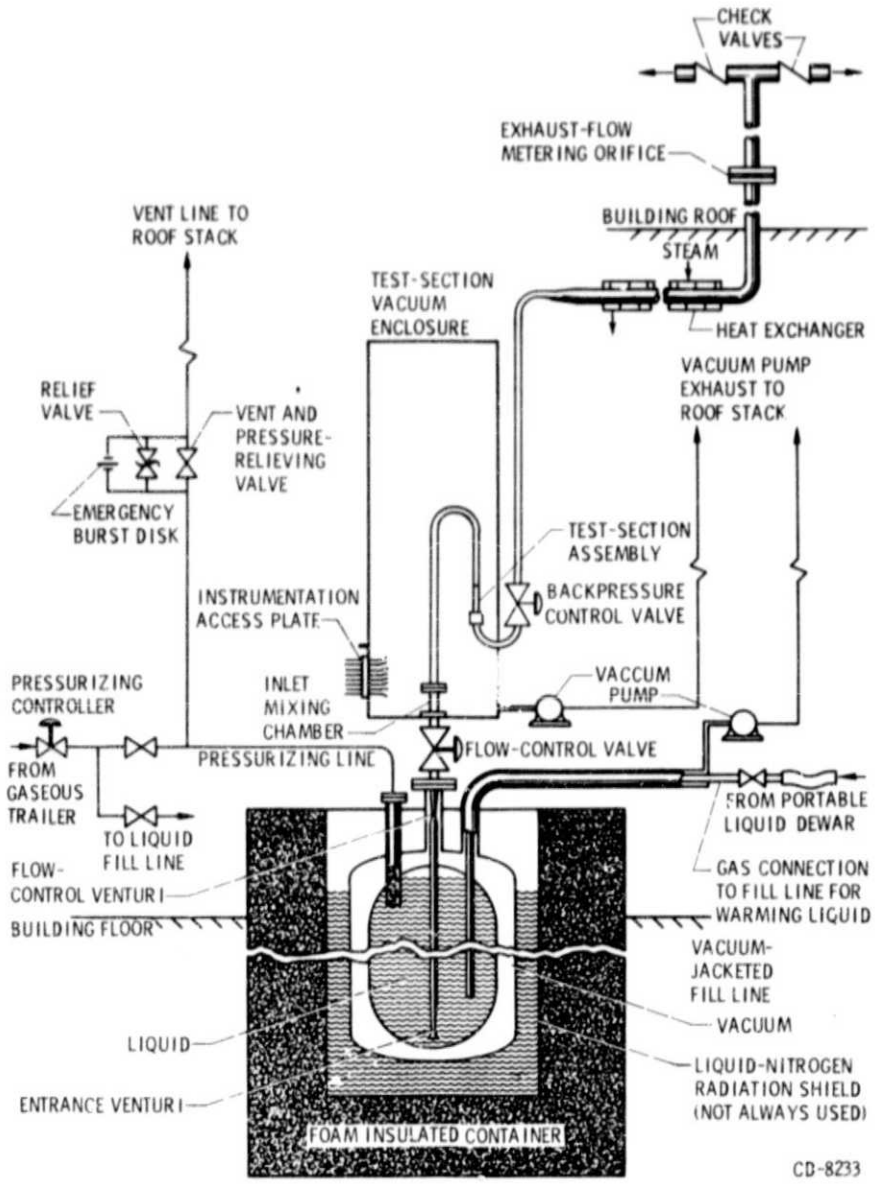

Figure 4. - Schematic diagram of high-pressure liquid-flow apparatus.

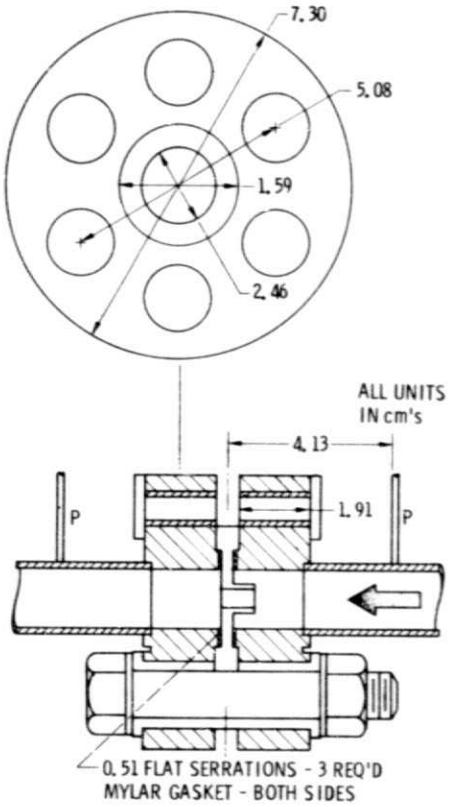

Figure 5. - Installation of Borda inlet - typical.

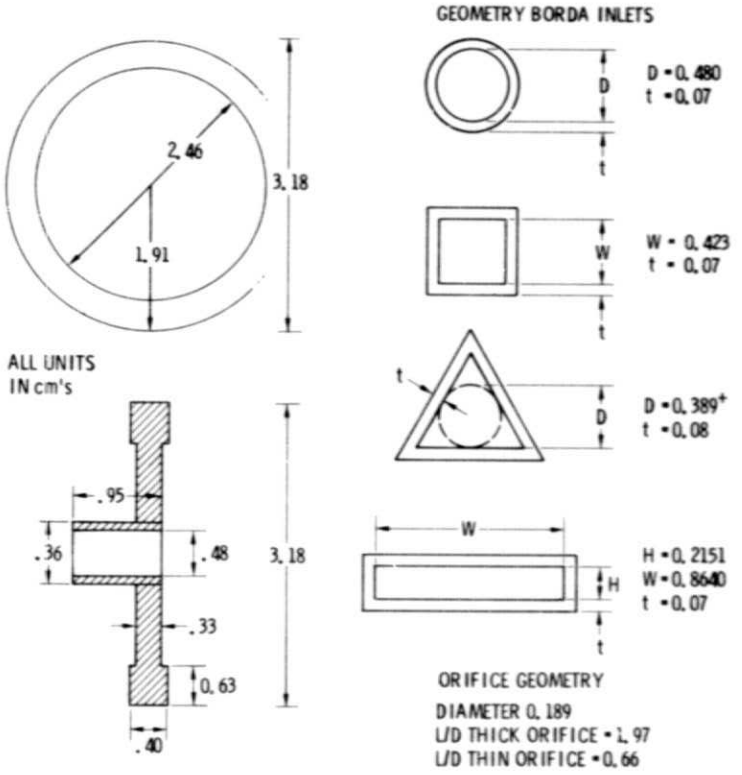

Figure 6. - Test section geometry - typical.

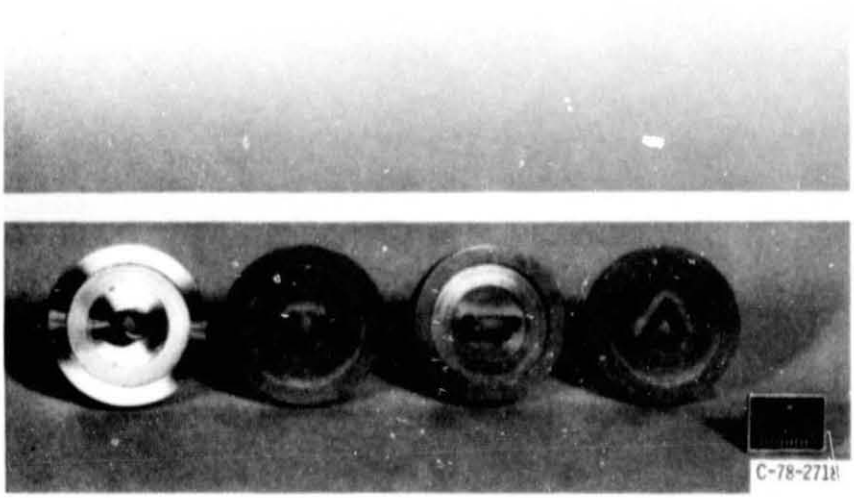

Figure 7. - Four Borda inlet configurations.

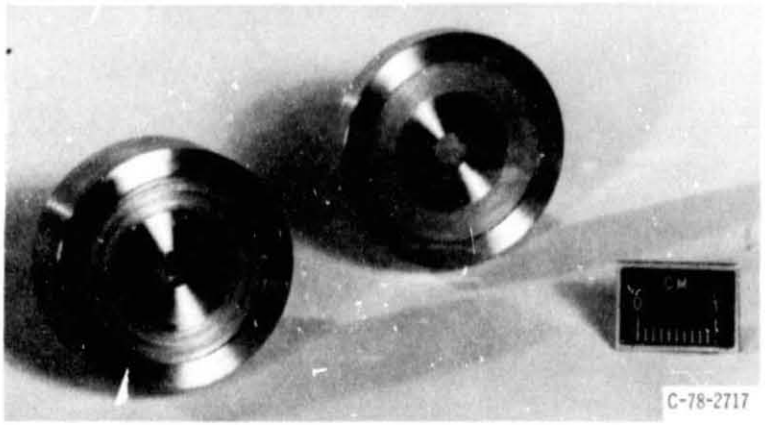

Figure 8. - Thick and thin orifices.

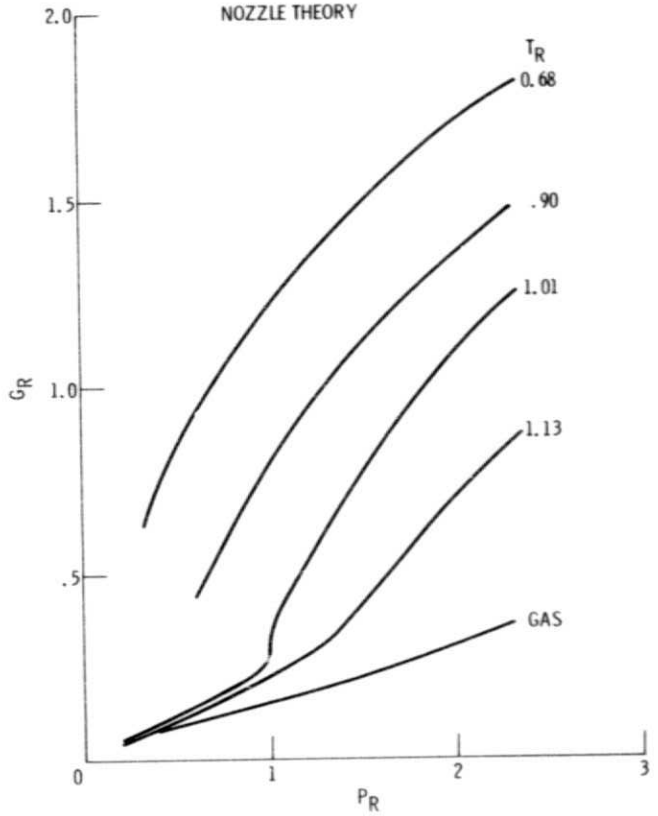

Figure 9. - Theoretical reduced mass flux for a nozzle.

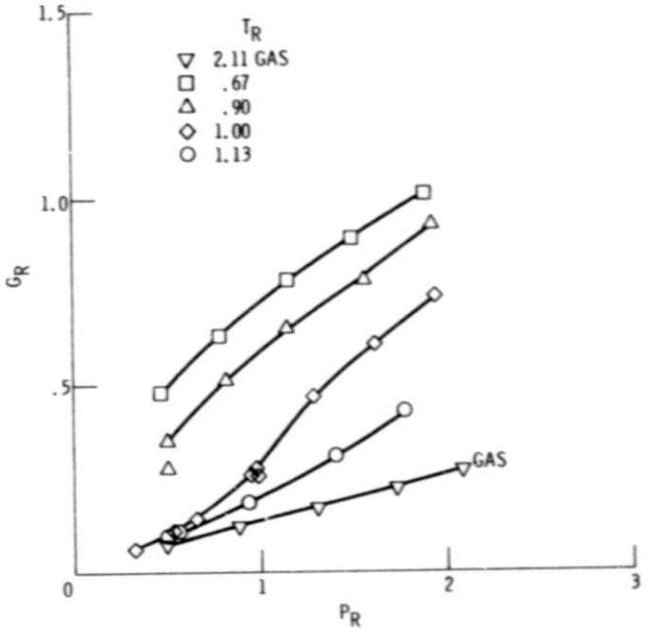

Figure 10. - Reduced mass flux as a function of reduced stagnation pressure - circular Borda inlet.

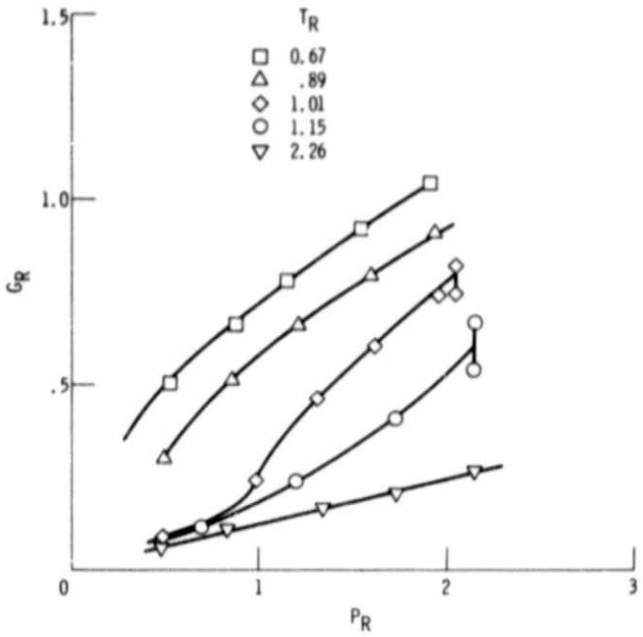

Figure 11. - Reduced mass flux vs reduced pressure for selected isotherms - square inlet Borda.

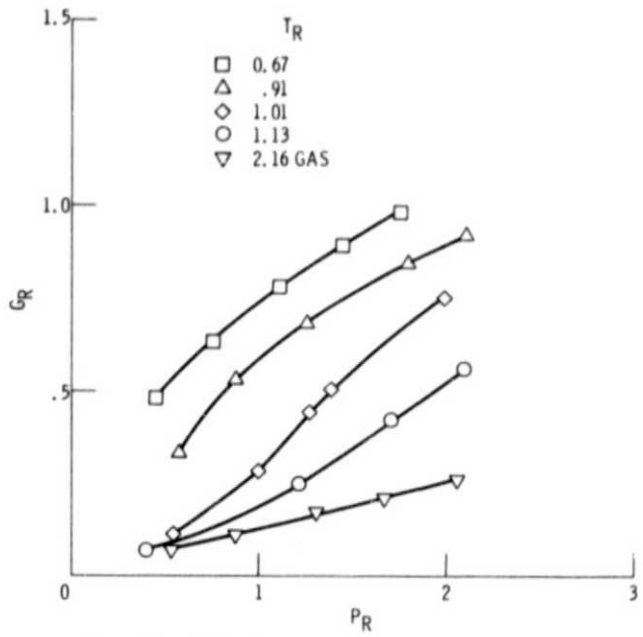

Figure 12. - Reduced mass flux vs reduced pressure for selected isotherms - triangular inlet Borda.

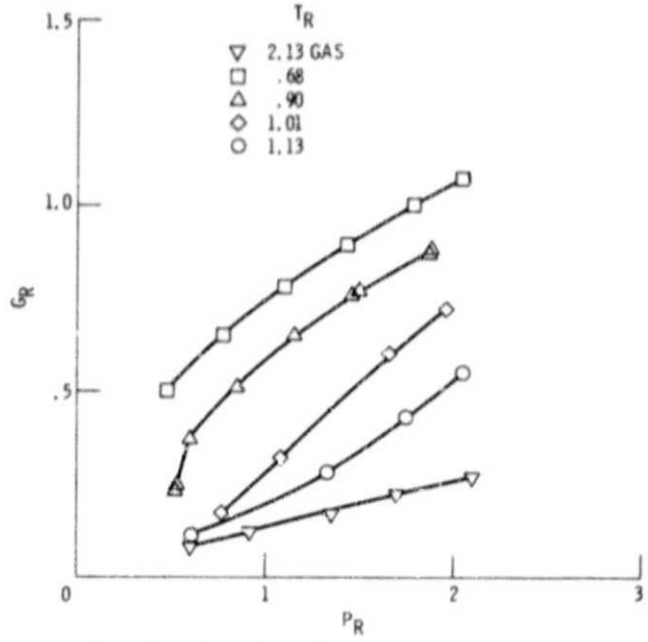

Figure 13. - Reduced mass flux vs reduced pressure for selected isotherms - rectangular inlet Borda.

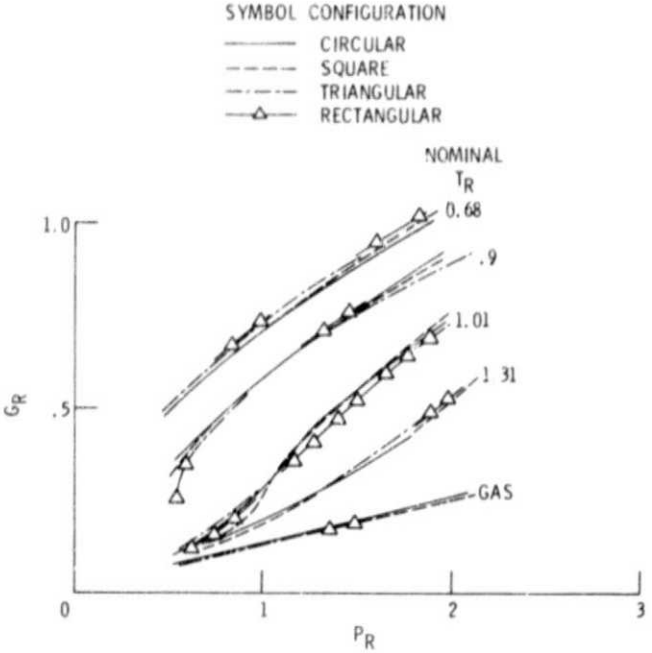

Figure 14. - A composite plot of reduced mass flux vs reduced pressure at selected isotherms for four Borda inlet geometries.

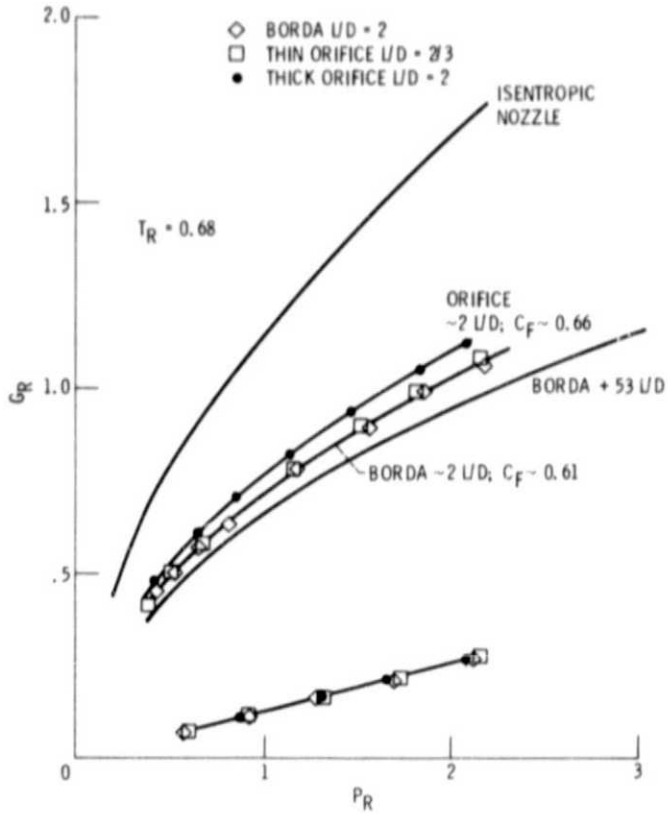

Figure 15. - Reduced mass flux vs reduced pressure for thick and thin orifices.

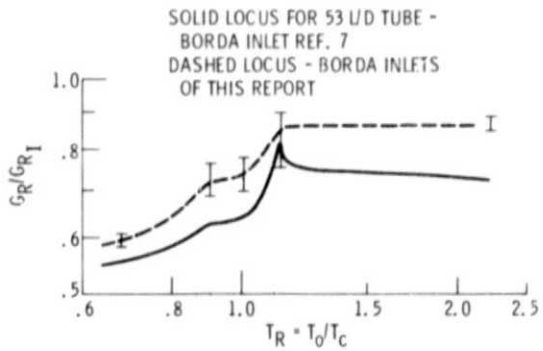

Figure 16. - Reduced flow rate ratio vs reduced temperature for fluid nitrogen.